



# Inorganic cesium lead halide CsPbX<sub>3</sub> nanowires for long-term stable solar cells

Jin-Feng Liao, Wen-Guang Li, Hua-Shang Rao, Bai-Xue Chen, Xu-Dong Wang, Hong-Yan Chen and Dai-Bin Kuang\*

**ABSTRACT** ABX<sub>3</sub>-type organic-inorganic hybrid halide perovskite materials have been recognized as promising candidates for optoelectronic applications. However, poor stability of organic-inorganic hybrid perovskite hinders their forward long-term utilization and hence an effective strategy is needed to replace the organic part with an inorganic cation. Herein, all inorganic CsPbI<sub>3</sub> nanowires with a diameter of 50–100 nm are synthesized on fluorine-doped tin oxide glass via a simple solution-dipping process, which are further transformed into CsPbBr<sub>3</sub> nanowires through a solution-phase halide exchange method. A phase change from non-perovskite to perovskite structure is observed during the ion substitution process of I<sup>-</sup> by Br<sup>-</sup>, which is elaborated by X-ray diffraction, absorption and photoluminescence spectra. We for the first time apply the as-formed CsPbI<sub>3</sub> and CsPbBr<sub>3</sub> nanowires into perovskite solar cells, yielding power conversion efficiency of 0.11% and 1.21%, respectively. The inorganic CsPbBr<sub>3</sub> nanowire solar cell shows impressive stability which still remains 99% of the initial power conversion efficiency even after 5500 h aging.

**Keywords:** inorganic perovskite, nanowires, ion exchange, solar cells, long-term stability

## INTRODUCTION

The past seven years have witnessed the rapid development of perovskite solar cells (PSCs), with the power conversion efficiency (PCE) rocketing to 22.1% [1] from the initial 3.8% [2], which strongly demonstrates that organic-inorganic hybrid halide perovskite (hybrid perovskite) is a family of promising materials for optoelectronic applications. Hybrid perovskites have been confirmed to possess numerous highly-appreciated properties, such as prominent sunlight absorption [3], long electron/hole diffusion lengths [4,5], ease and low cost fabrication [6], etc., which

render them an ideal candidate for various applications in light-emitting devices (LEDs) [7], semiconductor laser [8], and photodetectors [9].

However, hybrid perovskites are highly sensitive to moisture [10], ultraviolet (UV) light [11], and heat [12], which hinders their forward application [13,14]. Lead halides are the usual degradation product of the hybrid perovskites [10,15], deteriorating the performance of the solar cells, stemming from the wide bandgap and poor electrical conductivity [16,17]. Fortunately, inorganic perovskites, cesium lead halides (CsPbX<sub>3</sub>, X=Cl, Br, I) exhibit excellent compositional stability under thermal stress [18], among which CsPbBr<sub>3</sub> possesses an impressive humidity stability [19], showing promise on addressing those issues. Actually, pioneer work has already evidenced that CsPbX<sub>3</sub> (X=Br, I) perovskites also exhibit significant photoelectric properties. Perovskite CsPbBr<sub>3</sub> is a direct bandgap semiconductor with a bandgap of 2.3 eV [20] and is reported to possess not only a long electron lifetime of 2.5 μs but also a high electron mobility up to ~1000 cm<sup>2</sup> V<sup>-1</sup> s<sup>-1</sup> [21], which far outweighs that of single crystals of MAPbI<sub>3</sub> (24 cm<sup>2</sup> V<sup>-1</sup> s<sup>-1</sup>) [5]. Moreover, of particular note is that cesium halide perovskites greatly outperform hybrid perovskites in terms of stability. It has been demonstrated that PSCs based on CsPbBr<sub>3</sub> are more resistant to humidity and light illumination in comparison with MAPbBr<sub>3</sub> [19]. As for CsPbI<sub>3</sub>, the undesirable yellow phase (non-perovskite structure) is formed under ambient temperature [22] which shows only 0.09% in PCE due to an unfavorable wide bandgap [23].

Morphology control has been investigated to have significant effects on the photophysical and photochemical properties and it is highly recommended as a starting point to enhance the performance of the materials for optoelec-

MOE Key Laboratory of Bioinorganic and Synthetic Chemistry, School of Chemistry, Sun Yat-sen University, Guangzhou 510275, China

\* Corresponding author (email: kuangdb@mail.sysu.edu.cn)

tronic applications [24]. For instance, hybrid perovskites in the form of nanowires have been already synthesized and applied into PSCs [25], LEDs [26], laser [27] and photodetectors [28] etc., on account of the prominent properties of nanowires, such as fast electron transportation [29], direct charge transfer pathway [30] and low charge recombination [31]. However, limited attempts have been devoted to the controllable synthesis of all inorganic halide perovskites with well-defined nanostructure. Very recently, one dimensional  $\text{CsPbX}_3$  ( $X=\text{I}, \text{Br}, \text{Cl}$ ) nanowires [32] and quasi 2D nanoplates [33] were synthesized respectively by modifying the hot-injection technique reported by Protesescu *et al.* [34], where the as-formed  $\text{CsPbX}_3$  nanowires reveal temperature-dependent photoluminescence (PL) and the nanoplates present high photoluminescent quantum yields (PLQYs) up to 90%, both of which are deemed as ideal candidates for optoelectronic devices. However, it is well known that hot-injection technique requires rigorous experimental condition (high temperature, inert atmosphere) and the organic surfactant (oleic acid, oleylamine) bound to the surface is adverse to the charge carrier transportation [35,36], which leads to a foregoing purification step to remove such ligands before film fabrication. Moreover, it is still challenging to employ colloidal solution with specific morphology to assemble film on conductive substrate as a result of dissolution [35] and aggregation [37]. For this reason, it is of great significance to *in situ* synthesize all inorganic  $\text{CsPbX}_3$  nanowires on conductive substrate directly without the assistance of organic surfactant.

Herein, we report the synthesis of  $\text{CsPbI}_3$  and  $\text{CsPbBr}_3$  nanowires on fluorine-doped tin oxide (FTO) glasses by a simple solution-dipping process and solution-phase halide exchange method, respectively. Scanning electron microscopy (SEM), X-ray diffraction spectra (XRD), absorption spectra (UV-vis) and PL spectra were used to investigate the conversion process from  $\text{CsPbI}_3$  to  $\text{CsPbBr}_3$  nanowires. It is interesting to note such exchange by dipping the  $\text{CsPbI}_3$  nanowires/FTO glass into the methanol solution of  $\text{CsBr}$  and annealing at  $150^\circ\text{C}$  can not only induce the exchange of  $\text{I}^-$  to  $\text{Br}^-$ , but also result in the structure transformation from nonperovskite structure  $\text{CsPbI}_3$  to perovskite structure  $\text{CsPbBr}_3$ . After the complete anion exchange of  $\text{I}^-$  to  $\text{Br}^-$ , the photovoltaic performance of the planar PSCs based on  $\text{CsPbBr}_3$  nanowires is 10 times higher than that of  $\text{CsPbI}_3$  nanowires. Furthermore, the current inorganic  $\text{CsPbBr}_3$  nanowire solar cell shows excellent stability which remains 99% of the initial PCE even after 5500 h aging time at room temperature.

## EXPERIMENTAL SECTION

### Materials

Lead iodide ( $\text{PbI}_2$ ,  $\geq 98\%$ ), lead bromide ( $\text{PbBr}_2$ ,  $\geq 98\%$ ), 2, 2', 7, 7'-tetrakis-(*N, N*-di-*p*-methoxyphenylamine)-9, 9'-spirobifluorene (spiro-OMeTAD), bis(trifluoromethane) sulfonamide lithium salt (Li-TFSi), 4-*tert*-butylpyridine (*t*-BP), chlorobenzene and dimethylformamide (DMF, anhydrous, 99.8%) were purchased from Sigma-Aldrich. Cesium bromide ( $\text{CsBr}$ ,  $>99.9\%$ ), cesium iodide ( $\text{CsI}$ ,  $>99.9\%$ ) and hydroiodic acid (HI, 57% *w/w*) were purchased from Aladdin. Dried methanol and ethanol were purchased from Guangzhou Chemical Reagent factory.

### Synthesis of $\text{HPbI}_3$

$\text{HPbI}_3$  powders were synthesized according to a previously reported method [38] by dissolving  $\text{PbI}_2$  (9.26 g, 20 mmol) and 57% *w/w* hydroiodic acid (4 mL, 30 mmol) into 30 mL DMF with stirring at room temperature for 2 h. The solvent was removed by evaporating the resulting solution at  $60^\circ\text{C}$ , and the precipitate was washed with excess ethanol before dried under vacuum for 24 h.

### Synthesis of $\text{CsPbI}_3$ nanowires and $\text{CsPbBr}_3$ nanowires

Forty microliter of  $\text{HPbI}_3$  precursor solution ( $1 \text{ mol L}^{-1}$  dissolved in DMF) was firstly deposited onto FTO substrate by spin-coating at 5000 rpm for 60 s. This substrate was then dipped into a solution of  $10 \text{ mg mL}^{-1}$   $\text{CsI}$  in methanol to form yellow  $\text{CsPbI}_3$  nanowires. Subsequently, the  $\text{CsPbI}_3$  nanowires film grown on FTO glass was dipped into a methanol solution of  $10 \text{ mg mL}^{-1}$   $\text{CsBr}$  for different periods and then annealed at  $150^\circ\text{C}$  for 10 min. Here, all the  $\text{CsPbX}_3$  ( $X=\text{Br}, \text{I}$ ) samples were annealed at  $150^\circ\text{C}$  for 10 min except special explanation.

### Fabrication of perovskite solar cells

FTO glasses were pre-patterned with  $3 \text{ mol L}^{-1}$  HCl and zinc powder before cleaned with deionized water, alcohol, and acetone successively via ultrasonic process. A compact  $\text{TiO}_2$  layer was deposited on the FTO glass by spin-coating a colloidal  $\text{TiO}_2$  solution at 3000 rpm for 30 s and 5000 rpm for 60 s before annealed at  $500^\circ\text{C}$  for 1 h. The  $\text{TiO}_2$  colloid solution was prepared following our previous report [39]. After cooling down to room temperature, the compact  $\text{TiO}_2$  film was immersed into  $0.04 \text{ mol L}^{-1}$   $\text{TiCl}_4$  aqueous solution for 30 min at  $70^\circ\text{C}$  and then heated to  $500^\circ\text{C}$  for 30 min. And then an  $\text{HPbI}_3$  layer was prepared on the  $\text{TiO}_2$  coated FTO by spin-coating.  $\text{CsPbI}_3$  nanowires were obtained by

immersing the as-prepared HPbI<sub>3</sub> film into 10 mg mL<sup>-1</sup> CsI methanol solution for 1 min and then annealed at 150°C for 10 min. As for CsPbBr<sub>3</sub> nanowire, the halide exchange was performed by dipping the CsPbI<sub>3</sub> nanowires film into 10 mg mL<sup>-1</sup> CsBr solution in methanol for 5 min and then annealed at 150°C for 10 min. Then a hole-transport material solution consisting of spiro-OMeTAD (73.2 mg), Li-TFSi (9.1 mg) and *t*-BP (28.8 μL) and chlorobenzene (1 mL) was spin-coated onto the perovskite nanowires at 5000 rpm for 60 s. An Au layer with a thickness of 100 nm was deposited by magnetron sputtering.

### Characterizations

The XRD patterns were recorded on RigakuCo. X-ray powder diffractometer (Cu Kα radiation, λ=1.5418 Å). A UV-vis-NIR spectrophotometer (Shimadzu UV-3600) was employed to measure the UV-vis absorption spectra. The morphology and composition of the samples were measured using a scanning electron microscope (SU8010) and an energy dispersive X-ray detector (IXRF), respectively. PL (excitation at 325 nm) was measured with Edinburgh Instruments LTD (FLSP980). The photovoltaic performance of PSCs was recorded using Keithley 2400 source meter with a scan rate of 0.15 V s<sup>-1</sup> under one sun AM 1.5G (100 mW cm<sup>-2</sup>) illumination with a solar light simulator (Oriel, Model:91192) which was calibrated with an NREL standard Si solar cell. And the active area of the cell was defined as 0.16 cm<sup>2</sup>.

## RESULTS AND DISCUSSIONS

### Synthesis of CsPbI<sub>3</sub> nanowires

A simple and facile solution-dipping method was developed to synthesize the CsPbI<sub>3</sub> nanowires on FTO glass substrate. As schemed in Fig. 1a, the HPbI<sub>3</sub> solution was spin-coated onto the FTO substrate first, followed by dipping into CsI methanol solution to assemble CsPbI<sub>3</sub> nanowires film. The HPbI<sub>3</sub> precursor was synthesized via the reaction of PbI<sub>2</sub> and HI according to the previous report [38]. The XRD pattern (Fig. S1) shows that the peak of PbI<sub>2</sub> at 12.7° shifts to 11.5° after reaction with HI as a result of an increased interlayer distance [38], and the atomic ratio of I to Pb is about 3:1 determined by energy dispersive X-ray spectra (EDX, Table S1), further indicating the successful synthesis of HPbI<sub>3</sub>. Fig. 1b shows the morphology of the HPbI<sub>3</sub> film, which is constituted by discontinuous, large sized grains and this phenomenon was also found in a recent report [40]. After reaction with CsI, the parent HPbI<sub>3</sub> film turned yellow, and surprisingly, nanowires with diameters of 50–100 nm and lengths up to several micrometers tightly covered on the FTO glass could be observed (Fig. 1c and Fig. S2a). The XRD patterns of the products can be assigned to orthogonal phase CsPbI<sub>3</sub> (Fig. 2), with a non-perovskite structure (JCPDS Card No. 74-1970) [32].

### Importance of HPbI<sub>3</sub> precursor in synthesis of CsPbI<sub>3</sub> nanowires

It should be noted that the HPbI<sub>3</sub> precursor played a vital

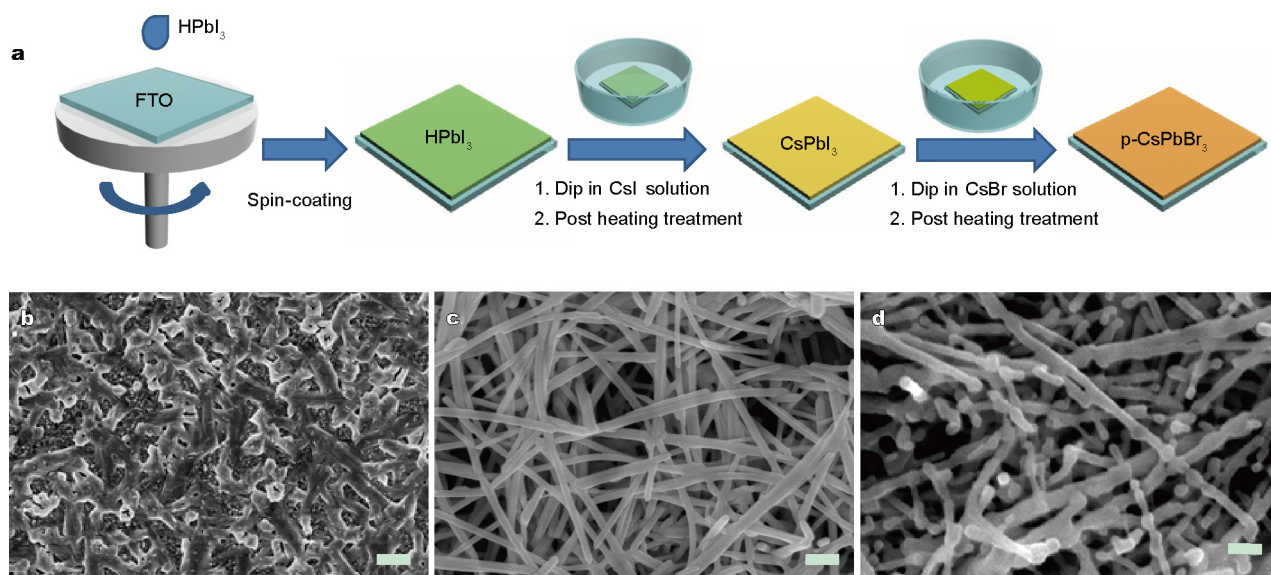


**Figure 1** (a) Schematic illustration of the synthesis of CsPbX<sub>3</sub> nanowires, and SEM images of (b) HPbI<sub>3</sub> films, (c) CsPbI<sub>3</sub> nanowires film, and (d) CsPbBr<sub>3</sub> nanowires film. Scale bars are 200 nm. The prefix p represents a perovskite structure.

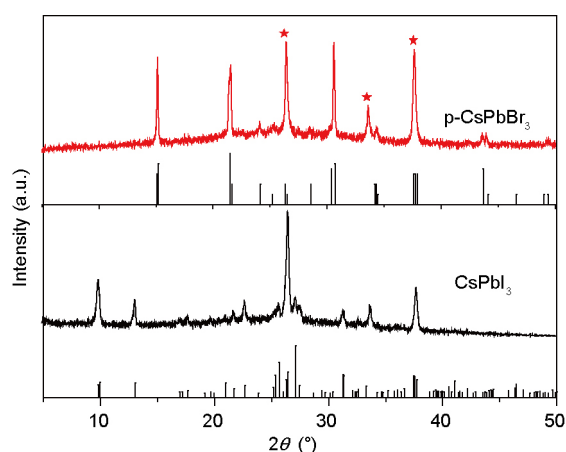


**Figure 2** XRD patterns of the as-formed CsPbI<sub>3</sub> nanowires by solution-dipping method and CsPbBr<sub>3</sub> obtained by halide exchange in comparison with standard XRD pattern. Peaks marked with an asterisk are XRD signals assigned to the FTO substrate.

role in the synthesis of CsPbI<sub>3</sub> nanowires. Attempt using the typical PbI<sub>2</sub> precursor film was conducted by dipping into CsI methanol solution. However, the XRD patterns (Fig. S3a) show that the peak of PbI<sub>2</sub> at 12.7° is still clearly observed after a long dipping time even though morphology of the obtained nanowires (Fig. S3b) indicates the incomplete conversion. In contrast, the reaction of HPbI<sub>3</sub> with CsI was astonishingly fast. CsPbI<sub>3</sub> was formed within 5 s and the XRD peak of HPbI<sub>3</sub> disappeared (Fig. S3c). Here, HPbI<sub>3</sub> having a faster complete reaction with CsI could be attributed to an increased layer lattice, which facilitated the reaction with CsI to form CsPbI<sub>3</sub> [38,40].

#### Synthesis of CsPbBr<sub>3</sub> nanowires via halide exchange

As mentioned above, nonperovskite CsPbI<sub>3</sub> is not beneficial for fabricating PSCs and it requires a high temperature (335°C) to convert to the black phase, which will revert to yellow phase after cooling down at ambient temperature [22]. Concerning that perovskite CsPbBr<sub>3</sub> possesses a superior stability than CsPbI<sub>3</sub> in ambient atmosphere, thus we look forward to converting the CsPbI<sub>3</sub> to CsPbBr<sub>3</sub> with the nanowires morphology maintained. The halide exchange process was performed by exposing the as-formed CsPbI<sub>3</sub> nanowires film into CsBr methanol solution and then annealed at 150°C for 10 min (Fig. 1a).

The accomplishment of the anion substitution of I<sup>-</sup> by Br<sup>-</sup> was accompanied by the color of the film turning to orange (CsPbBr<sub>3</sub>) from the inchoative pale yellow of CsPbI<sub>3</sub>. The XRD patterns in Fig. 2 confirm the formation of orthogonal phase CsPbBr<sub>3</sub>, with a perovskite structure

(JCPDS Card No. 72-7929) [19,32]. Highlighted in Fig. 1d and Fig. S2b, the CsPbBr<sub>3</sub> nanowires were successfully synthesized by anion exchange, with diameters merely changed to 50–200 nm. Compared with the CsPbI<sub>3</sub>, the CsPbBr<sub>3</sub> nanowires showed an uneven diameter and a rougher surface. The slight morphology variation is probably attributed to the crystal structural change from nonperovskite to perovskite structure during the halide exchange of I<sup>-</sup> by Br<sup>-</sup>. The PbI<sub>6</sub> octahedra are isolated in the nonperovskite CsPbI<sub>3</sub>, while PbBr<sub>6</sub> octahedra are connected in the perovskite CsPbBr<sub>3</sub> structure, which will be further discussed below. Cross-sectional SEM images (Fig. S4) illustrate the thickness variation between the as-prepared materials. The thickness of HPbI<sub>3</sub> film on FTO glass is ca. 300 nm (Fig. S4a), while after reaction with CsI, the thickness was almost doubled (Fig. S4b). Nevertheless, the thickness no longer changes during the Br substitution process (Fig. S4c).

The advent of ion substitution was proposed to figure out the difficulties in direct synthesis of materials with a specific morphology [41]. Here, an expectation of direct synthesis of CsPbBr<sub>3</sub> nanowires on FTO glass substrate was terminated by the trial of dipping the HPbI<sub>3</sub> film/FTO into a CsBr methanol solution straightly. XRD patterns (Fig. S5a) evidence the formation of perovskite structure CsPbBr<sub>3</sub> after dipping for 5 min, while the SEM image, presented in Fig. S5b indicates the morphology of cubes with a diameter of hundreds of nanometer was acquired instead of nanowires, which underlines the necessity of sacrificing the CsPbI<sub>3</sub> nanowires as templates for the sake of CsPbBr<sub>3</sub> nanowires.

#### Studies of anion exchange via XRD, UV-vis and PL

Anion exchange in cesium lead halide perovskite nanocrystals [42,43] has been demonstrated, while it has been rarely studied in bulk films [37]. To further gain insight into the ion exchange dynamics of the conversion reaction from CsPbI<sub>3</sub> to CsPbBr<sub>3</sub>, XRD patterns of the CsPbI<sub>3</sub> nanowires film as a function of dipping time into CsBr solution were measured. Fig. 3a indicates that, at the initial 20 s, no emerging XRD signals was detected, implying a similar crystallographic structure of nonperovskite CsPbI<sub>3</sub> was maintained but a magnification of XRD patterns (Fig. S6) showed that the XRD peaks of CsPbI<sub>3</sub> located at 9.9° and 13.1° were gradually shifted to higher angles at 10.1° and 13.3° with increasing dipping time respectively, indicating that I substituted by smaller atom Br and nonperovskite CsPbI<sub>3-x</sub>Br<sub>x</sub> was formed within such a short dipping time.

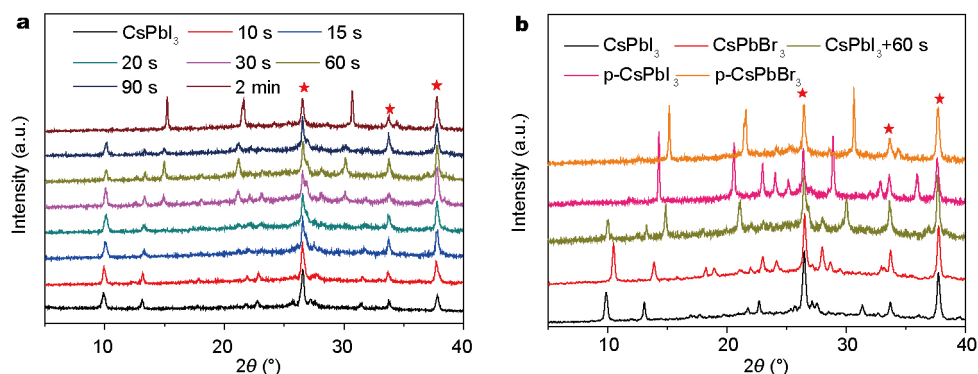


**Figure 3** (a) XRD pattern of CsPbI<sub>3</sub> nanowires film dipped in CsBr solution for varying time. (b) XRD pattern of the sample with dipping time of 60 s was compared with that of nonperovskite and perovskite CsPI<sub>3</sub> and CsPbBr<sub>3</sub>. Peak marked with an asterisk are XRD signals assigned to FTO substrate.

Extending the dipping time to 30 s till 90 s, several distinct emerging peaks at 14.9°, 21.1° and 30.1° could be easily observed. A further analysis by comparing CsBr solution for 60 s with that of both perovskite structure CsPbX<sub>3</sub> (X=I, Br) and nonperovskite structure CsPbX<sub>3</sub> (X=I, Br; Fig. 3b) suggested both two phases of CsPbI<sub>3-x</sub>Br<sub>x</sub> (perovskite structure and nonperovskite structure) coexisted since the XRD peaks of intermediate product stood at the middle of the corresponding peaks of CsPbI<sub>3</sub> and CsPbBr<sub>3</sub>. Whereafter, with dipping time increased to 2 min, a pure orthorhombic perovskite CsPbBr<sub>3</sub> was obtained, characterized with XRD patterns (Fig. 2) [19, 35]. Further prolonging the dipping time (e.g., >2 min) did not show any difference in XRD patterns (Fig. S7a), indicating the complete conversion of I<sup>-</sup> to Br<sup>-</sup>.

In order to explore the exact role of the post heat treatment in the aforementioned halide exchange process, we also measured XRD patterns of CsPbI<sub>3</sub> dipped in CsBr solution for varying time but without a post thermal treatment (Fig. S8a). The magnified of XRD patterns (Fig. S8b), reveal that the XRD signals of CsPbI<sub>3</sub> at 9.9° and 13.1° shifted to higher angles of 10.4° and 13.8° respectively after exposed to CsBr solution for 2 min, and no variations appeared to the XRD patterns as dipping process continued (Fig. S8c). Whereas, after the complete conversion, the color of the CsPbI<sub>3</sub> film turned from the initial yellow to white and the XRD patterns of the final white product can be assigned as orthorhombic CsPbBr<sub>3</sub> with a nonperovskite structure (Fig. S8d, JCPDS Card No. 74-2251), which is different from the results obtained by the halide process including a post heat treatment schemed in Fig. 1a. In addition, no XRD peaks of perovskite structure CsPbX<sub>3</sub> could be found during the ion substitution without a post heat treatment process (Fig. S8a), suggesting that the post

heat treatment was necessary to form the perovskite structure CsPbX<sub>3</sub>. In other words, the nonperovskite CsPbI<sub>3</sub> was transferred into the nonperovskite CsPbBr<sub>3</sub> after dipped into CsBr solution for 2 min, and a following post heat treatment (annealing at 150°C for 10 min) enabled the phase change from nonperovskite CsPbBr<sub>3</sub> to perovskite structure CsPbBr<sub>3</sub>, which was further proved by the temperature dependence XRD patterns of the as-formed nonperovskite structure CsPbBr<sub>3</sub> (Fig. S9). There is no variation in the XRD patterns until the temperature was raised to 150°C, and then the XRD peaks of perovskite CsPbBr<sub>3</sub> appeared while that of nonperovskite CsPbBr<sub>3</sub> disappeared.

As schemed in Fig. 4, we can make a conclusion for the halide exchange process including a post heat treatment, that nonperovskite CsPbI<sub>3-x</sub>Br<sub>x</sub> was formed within 30 s; both two phases of CsPbI<sub>3-x</sub>Br<sub>x</sub> (nonperovskite structure and perovskite structure) coexisted during 30–90 s; after 2 min the full conversion from CsPbI<sub>3</sub> to CsPbBr<sub>3</sub> was achieved with a phase change from initial nonperovskite to perovskite structure.

Transformation in crystal structure is always accompanied with photophysical properties variation [44]. In this regard, the absorption spectra of the CsPbI<sub>3</sub> nanowires films as a function of dipping time into CsBr methanol solution were characterized (Fig. 5a). The absorption onset of solution-phase synthesized CsPbI<sub>3</sub> nanowires locates at 449 nm with a bandgap of 2.78 eV from Tauc plot (Fig. S10), which matches well with the previous report [19]. After ion substitution completed, the as-formed CsPbBr<sub>3</sub> perovskite exhibited an absorption onset at 540 nm with a band gap of 2.30 eV. The rightmost blue solid line in Fig. 5a represents the absorption spectra of perovskite structure CsPbI<sub>3</sub> (obtained by heating the as-formed CsPbI<sub>3</sub> nano-

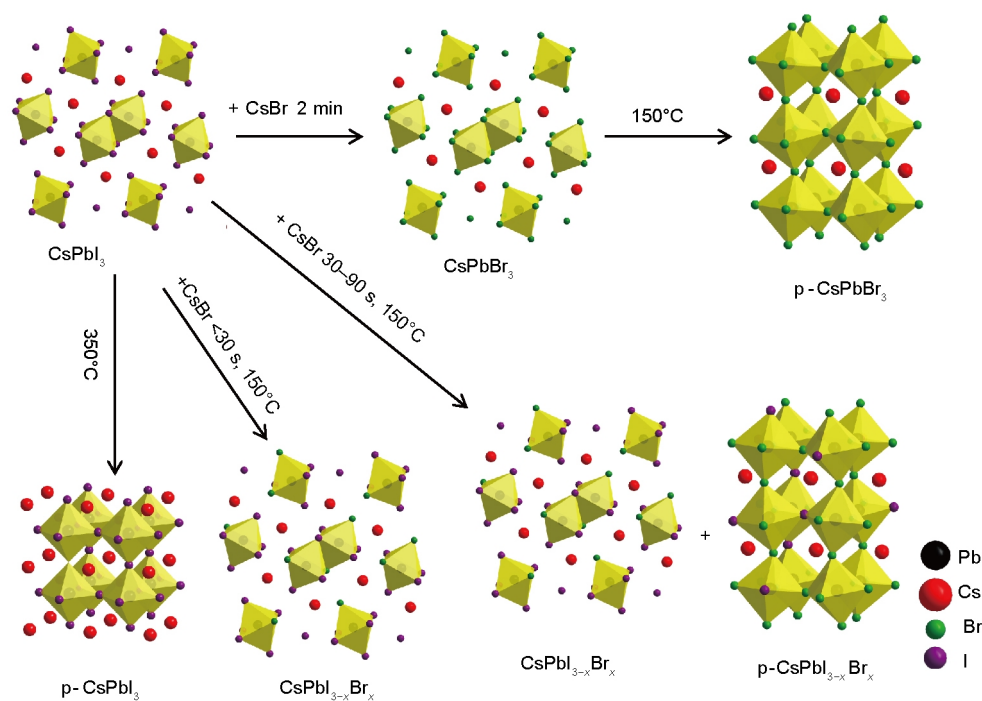


**Figure 4** The schematic diagram of structure conversion from nonperovskite CsPbI<sub>3</sub> to perovskite CsPbBr<sub>3</sub>.

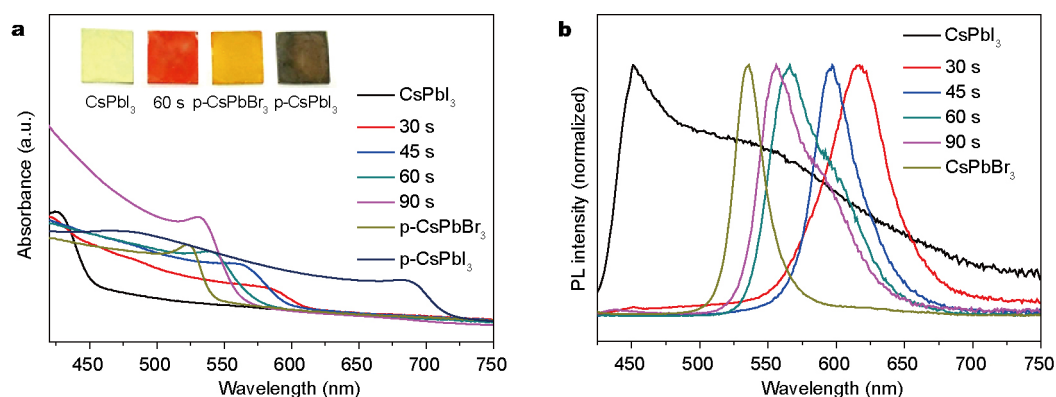


**Figure 5** (a) Absorption spectra and (b) normalized PL spectra of CsPbI<sub>3</sub> nanowires films dipped in CsBr solution for varying time. The inset photographs are CsPbI<sub>3</sub>, CsPbI<sub>3</sub> film with dipping time of 60 s, p-CsPbBr<sub>3</sub> and p-CsPbI<sub>3</sub> films from left to right, respectively.

wires film at 350°C) with an absorption onset at 700 nm and a bandgap of 1.7 eV (Fig. S10). It is interesting to note that the halide-exchange intermediate products (dipping time from 30 to 90 s) possess a wider absorption range than the initial material CsPbI<sub>3</sub> and the final product CsPbBr<sub>3</sub>. More specifically, after dipped in CsBr solution for 30 s, the absorption onset of the CsPbI<sub>3</sub> film shifts to around 615 nm, and towards to 600 nm (for 45 s), 581 nm (for 60 s) and 570 nm (for 90 s) gradually as I<sup>-</sup> substitution continued, and finally towards the onset of CsPbBr<sub>3</sub> 540 nm with the shift ceased as dipping time advances (Fig. S7b). Studies about CsPbX<sub>3</sub> nanocrystals halide exchange have illustrated that

the absorption onset of the perovskite structure CsPbI<sub>3-x</sub>Br<sub>x</sub> can be varied from 520–700 nm by adjusting the atom ratio of Br to I [42,43], and therefore it can be concluded that the perovskite structure CsPbI<sub>3-x</sub>Br<sub>x</sub> intermediate was formed, which is consistent with the aforementioned XRD analysis in Fig. 3b. The inset photographs in Fig. 5a display the color variation of the as-prepared CsPbI<sub>3</sub> nanowires film after dipping into CsBr solution or heat treatment. The pale yellow film was the as-prepared CsPbI<sub>3</sub> nanowires, and after dipped into CsBr solution for 60 s, the film was red as a result of the formation of perovskite CsPbI<sub>3-x</sub>Br<sub>x</sub> but the final product perovskite CsPbBr<sub>3</sub> nanowires was or-

ange and the black film was the perovskite  $\text{CsPbI}_3$  film. The above analysis demonstrated that perovskite structure  $\text{CsPbI}_{3-x}\text{Br}_x$  with a tunable bandgap can be formed via a careful control of the dipping time.

Corresponding to UV-vis, PL spectra also witnessed such interesting phenomenon in optical spectrum, as shown in Fig. 5b. The PL spectrum of the as-prepared  $\text{CsPbI}_3$  nanowires consists of two peaks centered at 450 and 540 nm. The narrow peak is assigned as the band edge emission while the broad peak has been previously attributed to the formation of self-trapped excitons [32]. The temperature-dependent PL spectra of  $\text{CsPbI}_3$  NWs in Fig. S11 reveal that the exciton emission peak of  $\text{CsPbI}_3$  red-shifts with increasing temperature from 100 to 298 K, which is consistent with the formation of self-trapped exciton which can produce strong electron-phonon coupling contribution to dictate band gap behavior [32]. Similar to the UV-vis spectra, as dipping time extending from 30 to 90 s, the PL peaks shift from 620 to 560 nm. The PL emission peak of the final product is located at 538 nm indicating the as-formed  $\text{CsPbBr}_3$  nanowires are PL active, with a narrow full-width of half maximum (FWHM) about 40 nm. Further prolonging the dipping time to more than 2 min, no differences between the PL peaks position are observed, indicating full halide exchange from  $\text{CsPbI}_3$  to  $\text{CsPbBr}_3$  (Fig. S7c).

### Photovoltaic performance of PSCs based on $\text{CsPbX}_3$ nanowires

The optoelectronic application of perovskite material is becoming a recent research hotspot. In this regard, the current *in-situ* growth of  $\text{CsPbI}_3$  and  $\text{CsPbBr}_3$  nanowires are further applied to the PSCs. To elucidate that such method has a favorable reproducibility, ten independent devices based on  $\text{CsPbI}_3$  and  $\text{CsPbBr}_3$  nanowires were measured, respectively (as shown in Fig. S12). Fig. 6a shows the current density-voltage curves of both solar cells based on  $\text{CsPbI}_3$  and  $\text{CsPbBr}_3$  nanowires. As listed in Table 1, the performance of device based on  $\text{CsPbI}_3$  yields a short circuit current density ( $J_{\text{SC}}$ ) of  $0.415 \text{ mA cm}^{-2}$ , an open circuit voltage ( $V_{\text{OC}}$ ) of 643 mV, a fill factor (FF) of 0.429, and a PCE of 0.11%. By contrast, the device based on  $\text{CsPbBr}_3$  nanowires formed by anion exchange achieves a  $J_{\text{SC}}$  of  $2.96 \text{ mA cm}^{-2}$ , a  $V_{\text{OC}}$  of 851 mV, an FF of 0.445 and a PCE of 1.21%. It is very interesting to note that more than tenfold enhancement in the PCE is achieved by the substitution of  $\text{I}^-$  by  $\text{Br}^-$ . The PCE of the devices based on  $\text{CsPbI}_{3-x}\text{Br}_x$  intermediate formed in the conversion process was measured with an inferior performance compared with pure  $\text{CsPbBr}_3$ , properly owing to the existence of nonperovskite counterpart serving as traps limiting the photovoltaic properties. Fig. 6b presents the cross-sectional SEM image of the device based on  $\text{CsPbBr}_3$  nano-

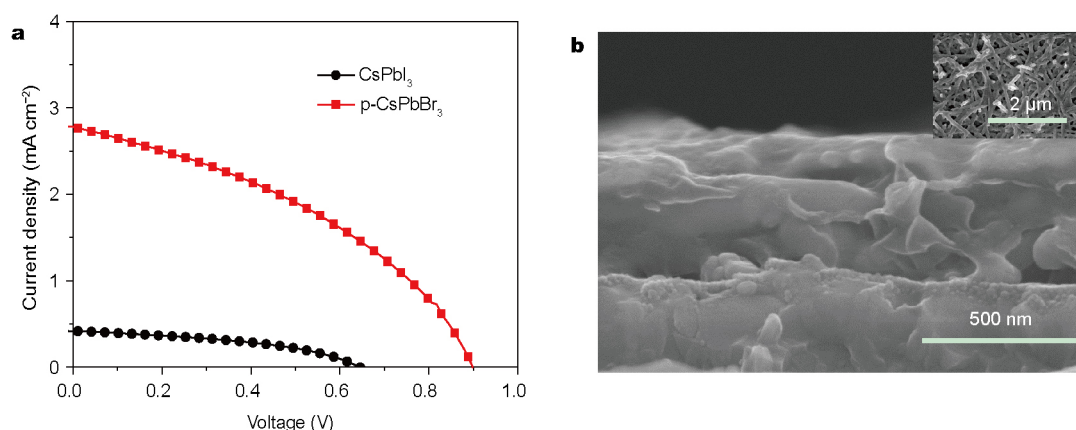


**Figure 6** (a)  $J$ - $V$  characteristics of the PSC devices and (b) cross-sectional and plane-view (inset image) SEM images of a full cell based on  $\text{CsPbBr}_3$  nanowires.

**Table 1** Device parameters of PSCs

	$J_{\text{SC}}$ ( $\text{mA cm}^{-2}$ )	$V_{\text{OC}}$ (mV)	PCE (%)	FF
$\text{CsPbI}_3$ nanowires	0.415	643	0.11	0.429
p- $\text{CsPbBr}_3$ nanowires	2.96	851	1.21	0.445

wires (FTO glass/ $\text{TiO}_2$  compact layer/ $\text{CsPbBr}_3$  nanowires/spiro-OMeTAD/Au) while the inset SEM image

in Fig. 6b is the plane-view image of the device based on CsPbBr<sub>3</sub>, where nanowires can be easily seen revealing that spiro-OMeTAD does not form a top layer upon the nanowires film but fills the empty space among nanowires, as does Au electrode. Moreover, there is no distinct layer boundary between the CsPbBr<sub>3</sub> nanowires with spiro-OMeTAD and Au electrode from the cross-sectional SEM image. Therefore, these inferior performances are mainly attributed to the insufficient coverage of the random CsPbX<sub>3</sub> nanowires on the substrate, which causes a direct contact between c-TiO<sub>2</sub> with spiro-OMeTAD or Au electrode resulting in the electron-hole recombination [45]. On the other hand, nanowires with an incomplete coverage on substrate will lead to a great loss in light harvesting, thus a decrease in  $J_{sc}$  [46]. For comparison, solar cells based on cube-based CsPbBr<sub>3</sub> films were fabricated with the same configuration. Table S2 summarized the photovoltaic metrics of 8 devices based on cubed-based CsPbBr<sub>3</sub> film with an average PCE of 0.14%, which is lower than that of CsPbBr<sub>3</sub> nanowires. By contrast, the better performance can be attributed to prominent properties of nanowires, such as fast electron transportation and direct charge transfer pathway.

#### Long-term stability of PSCs based on CsPbX<sub>3</sub> nanowires

The stability of solar cell is a crucial issue for the commercial application. Till today, the long-time stability of organic-inorganic PSC is still unsatisfactory and required to be resolved urgently. Herein, the stability study of the inorganic CsPbI<sub>3</sub> and CsPbBr<sub>3</sub> nanowire planar perovskite solar cell is further performed. Fig. 7 presents the normalized stability curves of both CsPbI<sub>3</sub> and CsPbBr<sub>3</sub> nanowire solar cells, which highlight that the current inorganic perovskite solar cells are highly stable even after around 5500 h aging at ambient condition in dark. Such impressive stability of inorganic perovskite nanowire solar cells will potentially stimulate the wide applications.

#### CONCLUSIONS

In summary, we reported a simple solution-dipping method and halide exchange technique to synthesize the CsPbI<sub>3</sub> and CsPbBr<sub>3</sub> nanowires grown on FTO glass, respectively. Herein, SEM, XRD patterns, UV-vis spectra and PL spectra studies reveal that the nonperovskite structure CsPbI<sub>3</sub> is transferred into nonperovskite structure CsPbI<sub>3-x</sub>Br<sub>x</sub> as the first step of the halide conversion, and then perovskite structure CsPbI<sub>3-x</sub>Br<sub>x</sub> appears together be-

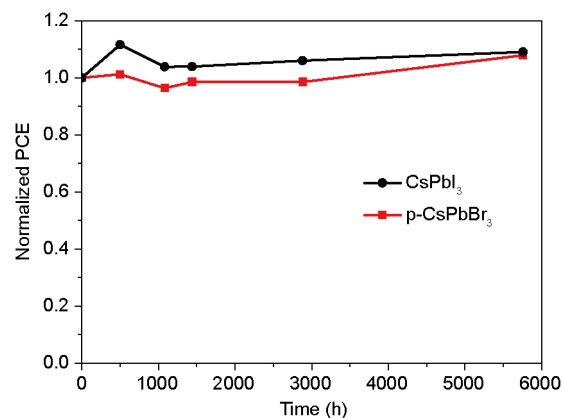


**Figure 7** Normalized PCE for devices based on CsPbI<sub>3</sub> and p-CsPbBr<sub>3</sub> nanowires as a function of aging time.

fore the complete conversion to perovskite structural CsPbBr<sub>3</sub>. PSC devices based on CsPbI<sub>3</sub> and CsPbBr<sub>3</sub> nanowires reached a PCE of 0.11% and 1.21%, respectively, and both exhibited impressive stability over 5500 h. Further studies on the thickness optimization of the CsPbX<sub>3</sub> nanowires and inorganic-organic hybrid MAPbX<sub>3</sub> nanowires are expected to obtain both high efficiency and good stability PSCs. Additionally, this work provides a simple solution-phase synthesis method to the *in situ* synthesis of the inorganic perovskite nanowires, which will stimulate the great potentials in semi-transparent perovskite solar cells, photodetectors and other optoelectronics.

Received 20 January 2017; accepted 24 February 2017;  
published online 14 March 2017

- 1 [http://www.nrel.gov/ncpv/images/efficiency\\_chart.png](http://www.nrel.gov/ncpv/images/efficiency_chart.png)
- 2 Kojima A, Teshima K, Shirai Y, *et al.* Organometal halide perovskites as visible-light sensitizers for photovoltaic cells. *J Am Chem Soc*, 2009, 131: 6050–6051
- 3 Im JH, Lee CR, Lee JW, *et al.* 6.5% efficient perovskite quantum-dot-sensitized solar cell. *Nanoscale*, 2011, 3: 4088–4093
- 4 Stranks SD, Eperon GE, Grancini G, *et al.* Electron-hole diffusion lengths exceeding 1 micrometer in an organometal trihalide perovskite absorber. *Science*, 2013, 342: 341–344
- 5 Dong Q, Fang Y, Shao Y, *et al.* Electron-hole diffusion lengths > 175 μm in solution-grown CH<sub>3</sub>NH<sub>3</sub>PbI<sub>3</sub> single crystals. *Science*, 2015, 347: 967–970
- 6 Chen BX, Rao HS, Li WG, *et al.* Achieving high-performance planar perovskite solar cell with Nb-doped TiO<sub>2</sub> compact layer by enhanced electron injection and efficient charge extraction. *J Mater Chem A*, 2016, 4: 5647–5653
- 7 Tan ZK, Moghaddam RS, Lai ML, *et al.* Bright light-emitting diodes based on organometal halide perovskite. *Nat Nanotech*, 2014, 9: 687–692



- 8 Xing G, Mathews N, Lim SS, *et al.* Low-temperature solution-processed wavelength-tunable perovskites for lasing. *Nat Mater*, 2014, 13: 476–480
- 9 Dou L, Yang YM, You J, *et al.* Solution-processed hybrid perovskite photodetectors with high detectivity. *Nat Commun*, 2014, 5: 5404
- 10 Li B, Fei C, Zheng K, *et al.* Constructing water-resistant  $\text{CH}_3\text{NH}_3\text{PbI}_3$  perovskite films via coordination interaction. *J Mater Chem A*, 2016, 4: 17018–17024
- 11 Leijtens T, Eperon GE, Pathak S, *et al.* Overcoming ultraviolet light instability of sensitized  $\text{TiO}_2$  with meso-superstructured organometal tri-halide perovskite solar cells. *Nat Commun*, 2013, 4: 2885
- 12 Conings B, Drijkoningen J, Gauquelin N, *et al.* Intrinsic thermal instability of methylammonium lead trihalide perovskite. *Adv Energ Mater*, 2015, 5: 1500477
- 13 Chen J, Liu D, Al-Marri MJ, *et al.* Photo-stability of  $\text{CsPbBr}_3$  perovskite quantum dots for optoelectronic application. *Sci China Mater*, 2016, 59: 719–727
- 14 Wei J, Shi C, Zhao Y, *et al.* Potentials and challenges towards application of perovskite solar cells. *Sci China Mater*, 2016, 59: 769–778
- 15 Niu G, Li W, Meng F, *et al.* Study on the stability of  $\text{CH}_3\text{NH}_3\text{PbI}_3$  films and the effect of post-modification by aluminum oxide in all-solid-state hybrid solar cells. *J Mater Chem A*, 2014, 2: 705–710
- 16 Berhe TA, Su WN, Chen CH, *et al.* Organometal halide perovskite solar cells: degradation and stability. *Energ Environ Sci*, 2016, 9: 323–356
- 17 Alberti A, Deretzi I, Pellegrino G, *et al.* Similar structural dynamics for the degradation of  $\text{CH}_3\text{NH}_3\text{PbI}_3$  in air and in vacuum. *ChemPhysChem*, 2015, 16: 3064–3071
- 18 Yantara N, Bhaumik S, Yan F, *et al.* Inorganic halide perovskites for efficient light-emitting diodes. *J Phys Chem Lett*, 2015, 6: 4360–4364
- 19 Kulbak M, Gupta S, Kedem N, *et al.* Cesium enhances long-term stability of lead bromide perovskite-based solar cells. *J Phys Chem Lett*, 2016, 7: 167–172
- 20 Kulbak M, Cahen D, Hodes G. How important is the organic part of lead halide perovskite photovoltaic cells? Efficient  $\text{CsPbBr}_3$  Cells. *J Phys Chem Lett*, 2015, 6: 2452–2456
- 21 Stoumpos CC, Malliakas CD, Peters JA, *et al.* Crystal growth of the perovskite semiconductor  $\text{CsPbBr}_3$ : a new material for high-energy radiation detection. *Cryst Growth Des*, 2013, 13: 2722–2727
- 22 Eperon GE, Paternò GM, Sutton RJ, *et al.* Inorganic cesium lead iodide perovskite solar cells. *J Mater Chem A*, 2015, 3: 19688–19695
- 23 Choi H, Jeong J, Kim HB, *et al.* Cesium-doped methylammonium lead iodide perovskite light absorber for hybrid solar cells. *Nano Energ*, 2014, 7: 80–85
- 24 Xu J, Yin J, Xiao L, *et al.* Bromide regulated film formation of  $\text{CH}_3\text{NH}_3\text{PbI}_3$  in low-pressure vapor-assisted deposition for efficient planar-heterojunction perovskite solar cells. *Sol Energ Mater Sol Cells*, 2016, 157: 1026–1037
- 25 Im JH, Luo J, Franckevičius M, *et al.* Nanowire perovskite solar cell. *Nano Lett*, 2015, 15: 2120–2126
- 26 Wong AB, Lai M, Eaton SW, *et al.* Growth and anion exchange conversion of  $\text{CH}_3\text{NH}_3\text{PbX}_3$  nanorod arrays for light-emitting diodes. *Nano Lett*, 2015, 15: 5519–5524
- 27 Zhu H, Fu Y, Meng F, *et al.* Lead halide perovskite nanowire lasers with low lasing thresholds and high quality factors. *Nat Mater*, 2015, 14: 636–642
- 28 Horváth E, Spina M, Szekrényes Z, *et al.* Nanowires of methylammonium lead iodide ( $\text{CH}_3\text{NH}_3\text{PbI}_3$ ) prepared by low temperature solution-mediated crystallization. *Nano Lett*, 2014, 14: 6761–6766
- 29 Liao JY, He JW, Xu H, *et al.* Effect of  $\text{TiO}_2$  morphology on photovoltaic performance of dye-sensitized solar cells: nanoparticles, nanofibers, hierarchical spheres and ellipsoid spheres. *J Mater Chem*, 2012, 22: 7910–7918
- 30 Wu WQ, Huang F, Chen D, *et al.* Thin films of dendritic anatase titania nanowires enable effective hole-blocking and efficient light-harvesting for high-performance mesoscopic perovskite solar cells. *Adv Funct Mater*, 2015, 25: 3264–3272
- 31 Xu YF, Wu WQ, Rao HS, *et al.*  $\text{CdS/CdSe}$  co-sensitized  $\text{TiO}_2$  nanowire-coated hollow spheres exceeding 6% photovoltaic performance. *Nano Energ*, 2015, 11: 621–630
- 32 Zhang D, Eaton SW, Yu Y, *et al.* Solution-phase synthesis of cesium lead halide perovskite nanowires. *J Am Chem Soc*, 2015, 137: 9230–9233
- 33 Bekenstein Y, Koscher BA, Eaton SW, *et al.* Highly luminescent colloidal nanoplates of perovskite cesium lead halide and their oriented assemblies. *J Am Chem Soc*, 2015, 137: 16008–16011
- 34 Protesescu L, Yakunin S, Bodnarchuk MI, *et al.* Nanocrystals of cesium lead halide perovskites ( $\text{CsPbX}_3$ , X = Cl, Br, and I): novel optoelectronic materials showing bright emission with wide color gamut. *Nano Lett*, 2015, 15: 3692–3696
- 35 Kim Y, Yassitepe E, Voznyy O, *et al.* Efficient luminescence from perovskite quantum dot solids. *ACS Appl Mater Interfaces*, 2015, 7: 25007–25013
- 36 Dastidar S, Egger DA, Tan LZ, *et al.* High chloride doping levels stabilize the perovskite phase of cesium lead iodide. *Nano Lett*, 2016, 16: 3563–3570
- 37 Hoffman JB, Schleper AL, Kamat PV. Transformation of sintered  $\text{CsPbBr}_3$  nanocrystals to cubic  $\text{CsPbI}_3$  and gradient  $\text{CsPbBr}_{x-1}\text{I}_3$  through halide exchange. *J Am Chem Soc*, 2016, 138: 8603–8611
- 38 Wang F, Yu H, Xu H, *et al.*  $\text{HPbI}_3$ : a new precursor compound for highly efficient solution-processed perovskite solar cells. *Adv Funct Mater*, 2015, 25: 1120–1126
- 39 Liao JY, Lei BX, Kuang DB, *et al.* Tri-functional hierarchical  $\text{TiO}_2$  spheres consisting of anatase nanorods and nanoparticles for high efficiency dye-sensitized solar cells. *Energ Environ Sci*, 2011, 4: 4079–4085
- 40 Pang S, Zhou Y, Wang Z, *et al.* Transformative evolution of organolead triiodide perovskite thin films from strong room-temperature solid-gas interaction between  $\text{HPbI}_3$ - $\text{CH}_3\text{NH}_2$  precursor pair. *J Am Chem Soc*, 2016, 138: 750–753
- 41 Eperon GE, Beck CE, Snaith HJ. Cation exchange for thin film lead iodide perovskite interconversion. *Mater Horiz*, 2016, 3: 63–71
- 42 Nedelcu G, Protesescu L, Yakunin S, *et al.* Fast anion-exchange in highly luminescent nanocrystals of cesium lead halide perovskites ( $\text{CsPbX}_3$ , X = Cl, Br, I). *Nano Lett*, 2015, 15: 5635–5640
- 43 Akkerman QA, D’Innocenzo V, Accornero S, *et al.* Tuning the optical properties of cesium lead halide perovskite nanocrystals by anion exchange reactions. *J Am Chem Soc*, 2015, 137: 10276–10281
- 44 Liao JF, Rao HS, Chen BX, *et al.* Dimension engineering on cesium lead iodide for efficient and stable perovskite solar cells. *J Mater Chem A*, 2017, 5: 2066–2072
- 45 Rao HS, Chen BX, Li WG, *et al.* Improving the extraction of photogenerated electrons with  $\text{SnO}_2$  nanocolloids for efficient planar perovskite solar cells. *Adv Funct Mater*, 2015, 25: 7200–7207
- 46 Ye T, Fu W, Wu J, *et al.* Single-crystalline lead halide perovskite arrays for solar cells. *J Mater Chem A*, 2016, 4: 1214–1217

**Acknowledgments** This work was supported by the National Natural Science Foundation of China (91433109 and 51472274), Guangdong Province Universities and Colleges Pearl River Scholar Funded Scheme (2016), the Program of Guangzhou Science and Technology

(201504010031), the Fundamental Research Funds for the Central Universities, and the Natural Science Foundation of Guangdong Province (S2013030013474 and 2014A030313148).

**Author contributions** Kuang DB and Liao JF designed the experiments. Liao JF performed the material synthesis, measurements, data analysis and prepared the manuscript. Li WG, Rao HS, Chen BX, Wang XD and Chen HY provided helps in the characterizations and revision of the manuscript. All authors contributed to the general discussion.

**Conflict of interest** The authors declare that they have no conflict of interest.

**Supplementary information** Experimental details are available in the online version of the paper.



**Jin-Feng Liao** is a PhD student at the School of Chemistry of Sun Yat-sen University (SYSU). She received her Bachelor's degree from Sun Yat-sen University in 2015. Now her current research interest focuses on all inorganic perovskite and its application in perovskite solar cells.



**Dai-Bin Kuang** is a professor at the School of Chemistry of SYSU. Dr. Kuang received his PhD degree from SYSU in 2003. He worked at Max Planck Institute of Colloids and Interfaces (Germany) from 2003 to 2004 and then at Ecole Polytechnique Fédérale de Lausanne (Switzerland) from 2004 to 2008 as a postdoctoral researcher. His current research interest is in the field of new energy materials, focusing on functional nanostructured materials and their application in dye-sensitized/quantum dot-sensitized solar cells, perovskite solar cells, photocatalysis and photoelectrochemical cells.

## 稳定的无机卤化铅铯纳米线钙钛矿电池

廖金凤, 李文广, 饶华商, 陈白雪, 王旭东, 陈洪燕, 匡代彬\*

**摘要** 有机无机杂化钙钛矿因其优异的光电性能受到广泛关注, 但是其对湿度、热的不稳定性会限制钙钛矿电池的进一步发展. 本文通过简单的溶液浸泡法在导电基底上制备了尺寸为50–100 nm的全无机碘化铅铯纳米线, 并通过离子交换法将碘化铅铯置换成溴化铅铯纳米线. 文章通过X射线衍射谱、紫外可见吸收光谱、荧光发光光谱对I离子交换成Br离子过程进行了研究. 结果发现I-Br离子交换过程中伴随着晶体结构的变化, 起初的碘化铅铯为非钙钛矿结构, 离子交换后制备的溴化铅铯为钙钛矿结构. 本文将全无机卤化铅铯纳米线应用在钙钛矿电池器件中, 器件显示出优越的稳定性, 放置5500小时效率几乎未衰减.